# Automatic AI-Driven Design of Mutual Coupling Reducing Topologies for Frequency Reconfigurable Antenna Arrays

Jiahao Zhang, Mobayode O. Akinsolu, Bo Liu, and Guy A. E. Vandenbosch

***Abstract*—An automatic AI-driven design procedure for mutual coupling reduction and a novel isolator are proposed for a frequency reconfigurable antenna array. The design process is driven and expedited by the parallel surrogate model-assisted differential evolution for antenna synthesis (PSADEA) method. The reconfigurable array element can switch its operation between the 2.5 GHz ISM band and the 3.4 GHz WiMAX band. By introducing the proposed isolator, the mutual coupling in the higher and lower band is reduced by 8 dB and 7 dB, respectively. The reconfigurable array was prototyped, and measurements agree well with simulations, verifying the validity of the proposed concept. Although used for a specific antenna in this communication, the proposed AI-driven design strategy is generic and can easily be employed for other array topologies.**

***Index Terms*—Mutual coupling reduction, reconfigurable antenna, frequency reconfigurability, surrogate modeling, optimization.**

## I. Introduction

With the development of modern wireless communication systems, multiple antenna technologies are becoming increasingly important [1], due to their ability to offer high gain, high resolution, beamforming, and beam scanning. When two or more antennas are placed next to each other on a single platform, they are mutually coupled in different ways depending on the type of antennas and their arrangement. For example, when two microstrip antennas are placed in proximity to each other, they couple to each other through the substrate/air layer (with the surface wave) and the air half-space (with the space wave). Typically, strong mutual coupling between antenna elements typically reduces the performance of any given multiple antenna system. Particularly, it causes scan blindness in phased arrays, limits the practical packing density of antenna arrays, and degrades the diversity performance of multiple-input multiple-output (MIMO) systems.

Mutual coupling reduction has been a topic of interest since the early days of antenna array design. The most commonly reported approaches include the use of: (1) defected ground structures (DGS) [2], [3], (2) electromagnetic band-gap (EBG) structures [4], [5], (3) soft surfaces [6], [7], (4) parasitic elements [8], [9], and (5) combinations of these [10]-[12].

Among these methods, the method of using parasitic elements has the clear advantage of resulting in a simple topology. The principle of using parasitic elements is to reduce mutual coupling by creating reverse coupling [13]. Antenna array configurations (antenna element topology, element spacing, etc.) tend to employ varying design processes for the parasitic elements. As a result, this process is quite dependent on the experience of the designers. Moreover, array configurations become more and more complicated in modern communication systems, involving multiband antennas, reconfigurable antennas and so on. In these cases, obtaining a design that reduces mutual coupling in a reasonable time becomes a great challenge. Therefore, it is an advantageous idea to propose a simple and generic mutual coupling reduction method for diverse array configurations serving complex applications, without requiring extensive experience from the designers.

Simulation-driven antenna designs have attracted attention in recent years. In [14] and [15], the performance of MIMO antennas was improved based on simulation-driven optimizations, considering mutual coupling levels. However, general mutual coupling reduction approaches were not explicitly investigated.

In this communication, a generic mutual coupling reduction method for diverse arrays is realized for the first time by introducing the concept of AI-driven design optimization or automation. Considering the requirements on generality, ability to obtain high-quality solutions for complex structures, and efficiency, the surrogate model-assisted global optimization technique is chosen. In particular, the parallel surrogate model-assisted differential evolution for antenna synthesis (PSADEA) method [16], [17] was employed. SADEA is an algorithm series dedicated to antenna optimization [16]-[19]. PSADEA is the latest method in this series. It offers a 3 to 20 times optimization efficiency improvement and a higher optimization ability compared to standard global optimization methods for practical antenna designs [16]-[19]. The essential features in PSADEA include the use of: (1) Gaussian process surrogate modeling, which is a kind of supervised learning technique for the prediction of the antenna performance, (2) complementary differential evolution search operators to explore the design space, (3) the reinforcement learning method to employ the search operators self-adaptively, and (4) the surrogate model-aware evolutionary search framework, which ensures the effective synergy of online surrogate modeling and global optimization.

In this communication, an automatic PSADEA-driven design of an innovative mutual-coupling-reducing parasitic element is proposed. The antenna topology considered is a dual-band frequency reconfigurable antenna, which can switch its operating band between the 2.5 GHz ISM band and the 3.4 GHz WiMAX band. With the resulting parasitic element, the mutual coupling in both bands is reduced to values below -20 dB. To the best knowledge of the authors, it is the first time that a mutual-coupling-reducing parasitic element is automatically designed based on machine learning and evolutionary computation. This procedure shows the advantages of generality, high design quality, and high efficiency without the need for reasonably good initial design parameters.

## II. PSADEA-Driven Design of Isolators

The mutual coupling reduction technique is illustrated in Fig. 1 for a two-element antenna array. Ant. 1 is excited by a current I. Through mutual coupling, a current αI is induced on Ant. 2, where α is the

Manuscript received January 22, 2020.

J. Zhang and G. A. E. Vandenbosch are with the ESAT-TELEMIC Research Division, Department of Electrical Engineering, KU Leuven, 3001 Leuven, Belgium (e-mail: jiahao.zhang@esat.kuleuven.be). M. O. Akinsolu is with the Faculty of Arts, Science and Technology, Wrexham Glyndwr University, Wrexham LL11 2AW, U.K. B. Liu is with James Watt School of Engineering, University of Glasgow, G12 8QQ, Scotland.

Color versions of one or more of the figures in this communication are available online at http://ieeexplore.ieee.org.

Digital Object Identifier

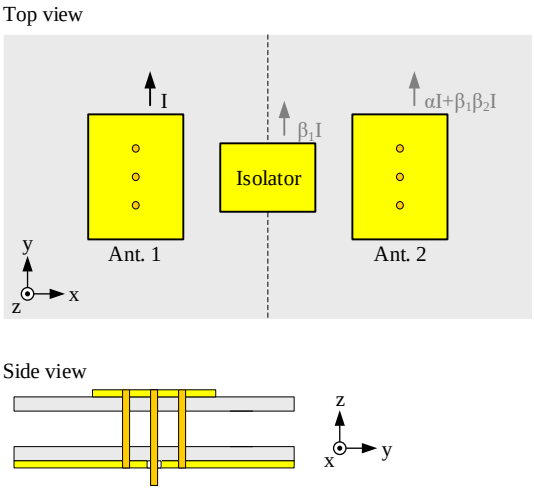


Fig. 1. Operation mechanism of the parasitic element-based mutual coupling reduction method. The detailed design of this array is given in Fig. 3.

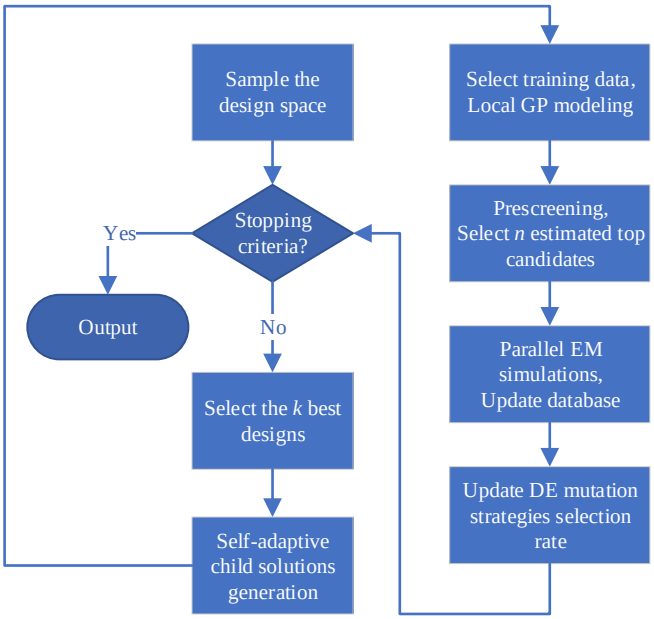


Fig. 2. PSADEA flow diagram.

coupling coefficient. By adding an isolator, a new situation is generated, the coupling situation of which can be worked out to the first order. Also, a current $\beta_1 I$ is now induced in the isolator, generating in its turn an induced current $\beta_1\beta_2 I$ in Ant. 2, where $\beta_1$ is the coupling coefficient between Ant. 1 and the isolator, and $\beta_2$ is the coupling coefficient between the isolator and Ant. 2. The total induced current in Ant. 2 then becomes $\alpha I + \beta_1\beta_2 I$. When the isolator is properly designed, the isolator creates reverse coupling, meaning that the total induced current approaches zero:

$$\alpha I + \beta_1\beta_2 I = 0 \quad (1)$$

The mutual coupling reduction mechanism shown in equation (1) clearly indicates that the design of the isolator is very dependent on the antenna and array topology, i.e., the coupling coefficient and the induced current. This design requirement triggered the demand for a general design strategy inspired by the AI-driven design automation. The advantage of using PSADEA in the design process via optimization is that isolators with complex and non-traditional topologies can be efficiently proposed to satisfy the condition in (1).

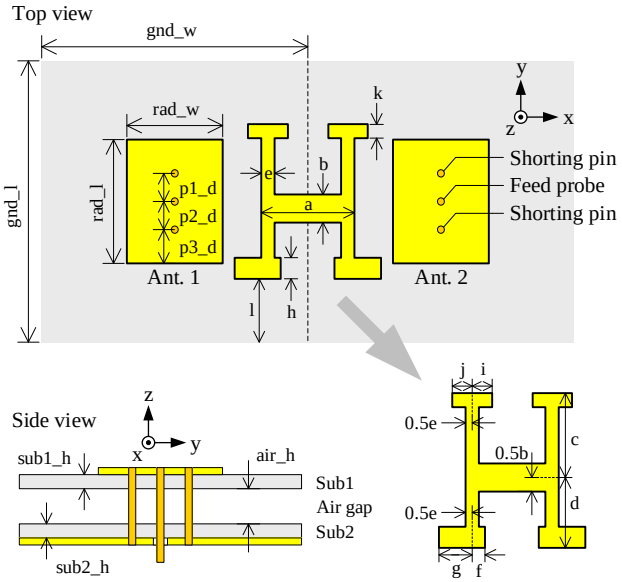


Fig. 3. The topology of the proposed isolator.

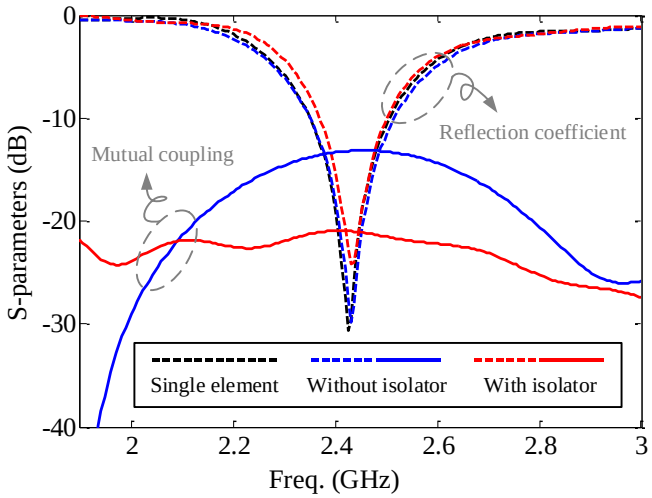


Fig. 4. S-parameters of Design 1. The dashed lines indicate reflection coefficients, the solid lines indicate the mutual coupling.

As shown in Fig. 2, PSADEA is initialized using a small number of samples from the design space. In each iteration, child solutions are generated by applying three types of DE mutation operators self-adaptively to a fixed number ($k$) of top-ranked candidate solutions. The self-adaptiveness comes from the fact that the probability to employ each DE mutation operator is related to the number of cases that, using such a mutation strategy, generate better solutions than the best-so-far solution. Gaussian process surrogate models are then constructed for each candidate in each child population using the nearest designs (based on Euclidean distance) from the database and their performance values as the training data points. The generated child solutions are prescreened to cope with the prediction uncertainty. The selected best solutions ($n$) are then simulated in parallel. More details can be found in [16]. All simulations reported in this communication were executed on a workstation with an Intel 8-core i9-9900K 3.6 GHz CPU and a 64 GB RAM and the time consumptions are wall clock time.

## III. ZOR Element at 2.5 GHz & 3.5 GHz

This general technique is worked out for an array of two zeroth-order-resonant (ZOR) antenna elements with an

TABLE I
PARAMETERS OF THE ZOR ANTENNA ARRAY

| Parameters | Design 1 | Design 2 | Parameters | Design 1 | Design 2 |
|---|---|---|---|---|---|
| gnd_w | 60 | 43 | p1_d | 6.13 | 4.08 |
| gnd_l | 60 | 43 | p2_d | 6.13 | 4.08 |
| rad_w | 22 | 14 | p3_d | 6.13 | 4.08 |
| rad_l | 24.5 | 16.3 | sub1_h | 0.8 | 0.8 |
| air_h | 5 | 4 | sub2_h | 0.8 | 0.8 |

All dimensions are in mm.

TABLE II
PARAMETERS OF THE PROPOSED ISOLATOR

| Parameters | Design 1 | | Design 2 | |
|---|---|---|---|---|
| | Range | Value | Range | Value |
| a | 0-38 | 30.06 | 0-29 | 16.46 |
| b | 0-20 | 4.26 | 0-15 | 2.85 |
| c | 0-30 | 18.76 | 0-20 | 14.99 |
| d | 0-30 | 5.61 | 0-20 | 19.45 |
| e | 0-10 | 6.84 | 0-10 | 8.90 |
| f | 0-10 | 0.77 | 0-10 | 7.92 |
| g | 0-10 | 6.98 | 0-10 | 5.97 |
| h | 0-20 | 5.64 | 0-15 | 9.32 |
| i | 0-10 | 4.31 | 0-10 | 1.02 |
| j | 0-10 | 1.62 | 0-10 | 9.16 |
| k | 0-20 | 10.79 | 0-15 | 10.90 |
| l | 0-50 | 11.29 | 0-40 | 2.39 |

All dimensions are in mm.

TABLE III
CONSTRAINTS AND TARGETS

| Constraints | | Targets | |
|---|---|---|---|
| Design 1 | Design 2 | Design 1 (2.4-2.5 GHz) | Design 2 (3.4-3.5 GHz) |
| a+2j-e<38 | a+2j-e<29 | S11<-10 dB | S11<-10 dB |
| a+2g-e<38 | a+2g-e<29 | S22<-10 dB | S22<-10 dB |
| c+d+l<60 | c+d+l<43 | S21<-20 dB | S21<-20 dB |

All dimensions are in mm.

omni-directional radiation pattern in the 2.5 GHz ISM band (Design 1). The topology and dimensions of these elements can be found in Fig. 3 and Table I. The shorting pins also serve to achieve omnidirectional radiation patterns [1]. FR4 substrates with permittivity 4.4 and loss tangent 0.009 are used. When the two antenna elements are placed at a distance of 0.5 λ at 2.5 GHz, the mutual coupling is around -13 dB, see Fig. 4. A complex H-shaped isolator with 12 dimensional parameters (a-l) is proposed, see Fig. 3. Note that some parameters, e.g., c, d, are defined as starting from the center of b, see the zoomed-in figure in Fig. 3. This implies that, when the values of c and/or d are smaller than 0.5b, the stub whose dimensions are controlled by c and/or d becomes overlapped and hidden in the geometry. The initial tuning range of these parameters can be set very wide, see Table II. In other words, the designers do not need to put much effort and experience into choosing good initial dimensions for the H-shaped topology. The reason is that the PSADEA method is used in the optimization. The constraints and targets of this optimization are given in Table III. The main idea when setting the constraints is to restrict the isolator inside the array footprint, and to keep the isolator clear from the radiators. After 137 parallel EM simulations (3 designs in parallel in each iteration), an optimized isolator was automatically obtained. The overall design

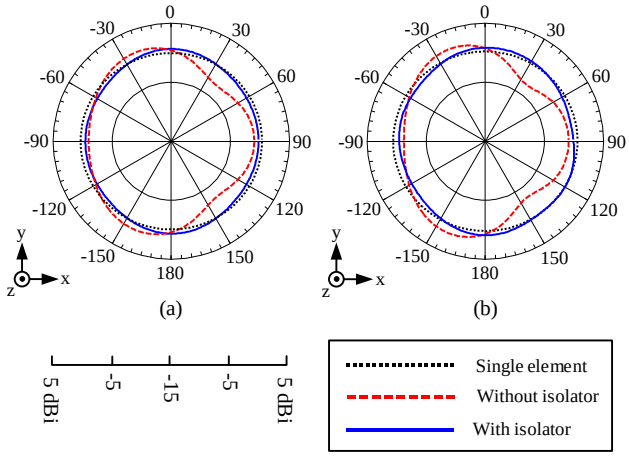


Fig. 5. Radiation patterns of (a) Design 1, (b) Design 2. (Abs values of the farfield directivity.)

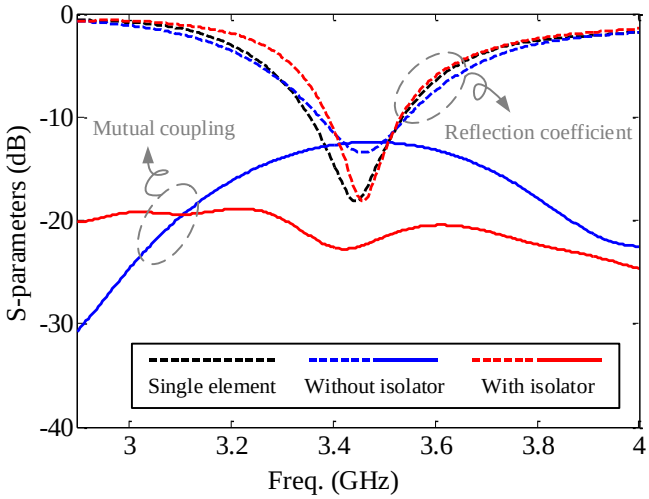


Fig. 6. S-parameters of Design 2. The dashed lines indicate reflection coefficients, the solid lines indicate mutual coupling.

time was about 9.1 hours. The simulated S-parameters are given in Fig. 4. The reflection coefficient covers the desired 2.4-2.5 GHz band, and the mutual coupling is reduced to below -20 dB. The array performance is summarized in Table IV.

The radiation patterns in the xy plane (H-plane) are shown in Fig. 5 (a). The single ZOR antenna element has an omnidirectional radiation pattern in the xy plane. The radiation pattern of the embedded element in the original two-element array is obviously distorted because of the mutual coupling effect. By introducing the proposed isolator, the radiation pattern of the embedded element (with isolator) becomes more similar to the one of the single element.

It has to be emphasized that the proposed method can easily be generalized to many other antenna element types and array configurations, for example, conventional microstrip antenna arrays (with single layer printed circuit board (PCB)), conventional air-gapped microstrip antenna arrays, conventional circular patch antenna arrays, etc. The designers only need to simply adjust the initial ranges and constraints of the isolator and the optimization targets according to the chosen element. For example, a smaller element results in narrower ranges. An additional Design 2 is provided to validate this fact. The ZOR antenna topology remains unchanged and the layout is still represented by Fig. 3, However, the dimensions are changed and provided in Table I. Note that the same isolator is used, and the design process is repeated with new ranges, constraints, and

TABLE IV
ARRAY PERFORMANCE

| | | Band (GHz) | S21 (dB) | Directivity (dBi) | Efficiency (%) |
|---|---|---|---|---|---|
| Design 1 | Single element | 2.35-2.50 | N/A | 1.16 | 0.86 |
| | Without isolator | 2.35-2.52 | -13.1 | 2.74 | 0.88 |
| | With isolator | 2.37-2.50 | -20.9 | 2.33 | 0.88 |
| Design 2 | Single element | 3.36-3.54 | N/A | 1.22 | 0.89 |
| | Without isolator | 3.38-3.54 | -12.4 | 3.07 | 0.90 |
| | With isolator | 3.39-3.53 | -21.1 | 2.31 | 0.89 |

TABLE VI
CONSTRAINTS AND TARGETS

| Constrains | Targets | | |
|---|---|---|---|
| | State | Freq. | Goal |
| a1+2j1-e1<16 | State 1 substrate=2.4 | 2.4-2.5 GHz | S11<-10 dB |
| a1+2g1-e1<16 | | 2.4-2.5 GHz | S22<-10 dB |
| c1+d1+l1<38 | | 2.4-2.5 GHz | S21<-20 dB |
| c2+d2+l2<38 | State 2 substrate=1.2 | 3.3-3.4 GHz | S11<-10 dB |
| | | 3.3-3.4 GHz | S22<-10 dB |
| | | 3.3-3.4 GHz | S21<-20 dB |

All dimensions are in mm.

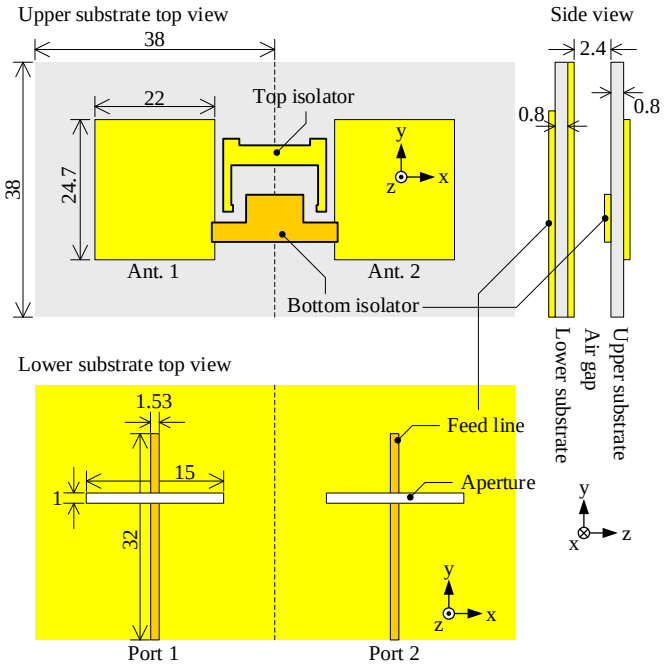


Fig. 7. Topology of the frequency reconfigurable antenna array with isolator.

targets, see Table II and Table III. After 30 parallel EM simulations (3 designs in parallel in each iteration), the targets were successfully reached, see the S-parameter results in Fig. 6. The radiation patterns are shown in Fig. 5 (b). The overall design time was about 2.5 hours. The optimized design parameters are given in Table II, and the antenna array performance is summarized in Table IV. Note that in comparison with the search ranges and constraints for the original Design 1 in Tables II and III, the search ranges and the constraints for the new Design 2 have simply been scaled down according to the dimensions of the new case.

TABLE V
PARAMETERS OF THE PROPOSED ISOLATOR

| Parameter | Range | Value | Parameter | Range | Value |
|---|---|---|---|---|---|
| a1 | 0-16 | 13.29 | a2 | 0-16 | 8.18 |
| b1 | 0-20 | 3.74 | b2 | 0-20 | 3.11 |
| c1 | 0-20 | 2.21 | c2 | 0-20 | 1.06 |
| d1 | 0-20 | 6.57 | d2 | 0-20 | 6.36 |
| e1 | 0-10 | 0.99 | e2 | 0-10 | 7.45 |
| f1 | 0-10 | 0.62 | f2 | 0-10 | 5.35 |
| g1 | 0-10 | 0.34 | g2 | 0-10 | 9.19 |
| h1 | 0-10 | 0.64 | h2 | 0-10 | 3.64 |
| i1 | 0-10 | 0.64 | i2 | 0-10 | 1.92 |
| j1 | 0-10 | 0.38 | j2 | 0-10 | 1.93 |
| k1 | 0-10 | 2.52 | k2 | 0-10 | 1.87 |
| l1 | 0-30 | 17.38 | l2 | 0-30 | 12.44 |

All dimensions are in mm.

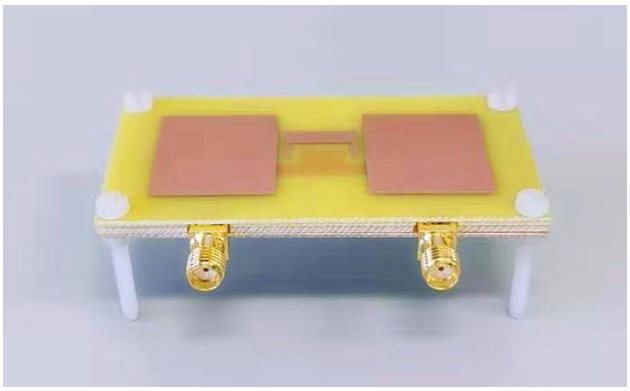

Fig. 8. Prototype of the proposed frequency reconfigurable antenna array.

## IV. DUAL-BAND FREQUENCY RECONFIGURABLE ELEMENT

In this section a more complex frequency reconfigurable antenna element is considered, as shown in Fig. 7. The radiator of the antenna is printed on the top layer of the upper substrate. The ground (with aperture) lies on the top layer of the lower substrate. The feed line is on the bottom layer of the lower substrate. By manually (mechanically) inserting different substrates to modify the equivalent permittivity of the aperture-coupled antenna element, the resonant frequency can be reconfigured. Note that the study of this reconfigurability is not the topic of study of this communication. This case is specifically used as a quite challenging example to illustrate the generality of the proposed mutual coupling reduction concept. However, although the reconfiguration of course cannot be done during operation of the antenna, it is still a solution in cases where one of the bands has to be pre-selected before installation after which it is kept fixed during operation. For state 1, the inserted substrate has a thickness of 2.4 mm, resulting in an operational frequency in the 2.5 GHz ISM band. For state 2, the thickness is 1.2 mm, resulting in an operational frequency in the 3.4 GHz WiMAX band. FR4 substrates with a permittivity of 4.4, and a loss tangent of 0.009 were used. For state 1, two FR4 substrates with a thickness of 1.6 mm and 0.8 mm can be stacked forming the 2.4 mm substrate. For state 2, two FR4 substrates with a thickness of 0.8 mm and 0.4 mm can be stacked to form the 1.2 mm substrate. The element spacing is 0.43 λ at 3.4 GHz. A dual-band isolator for this frequency reconfigurable antenna array is needed. Two H-shaped

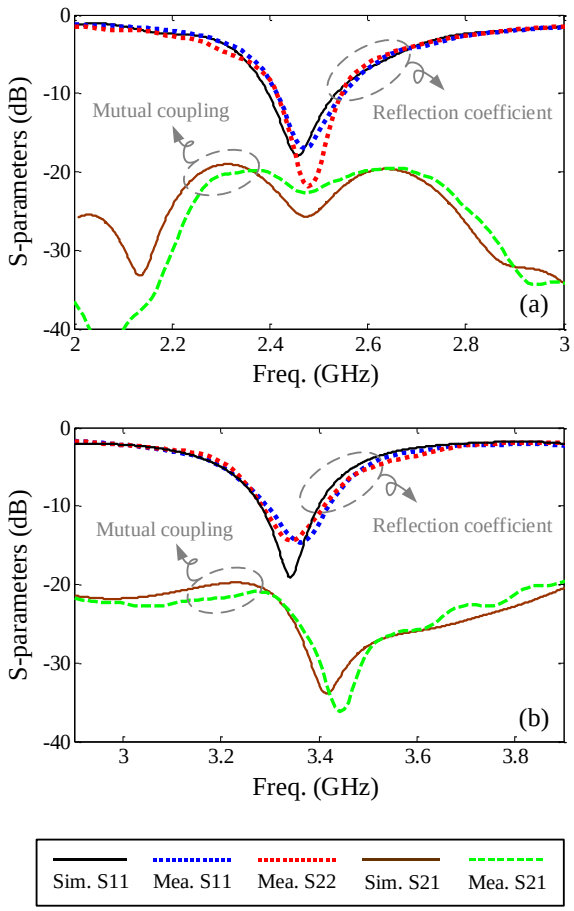


Fig. 9. S-parameters of the frequency reconfigurable antenna array. (a) State 1, (b) State 2. The dashed lines indicate the measurement results, the solid lines indicate the simulation results.

TABLE VII
ARRAY PERFORMANCE

| | | | S11 band (GHz) | S22 band (GHz) | S21 (dB) |
|---|---|---|---|---|---|
| State 1 | Single element | Sim. | 2.37-2.51 | 2.37-2.51 | N/A |
| | Without isolator | Sim. | 2.41-2.51 | 2.41-2.51 | -12.6 |
| | With isolator | Sim. | 2.40-2.54 | 2.40-2.54 | -21.3 |
| | | Mea. | 2.41-2.55 | 2.41-2.55 | -20.6 |
| State 2 | Single element | Sim. | 3.25-3.40 | 3.25-3.40 | N/A |
| | Without isolator | Sim. | 3.27-3.40 | 3.27-3.40 | -14.4 |
| | With isolator | Sim. | 3.28-3.40 | 3.28-3.40 | -20.3 |
| | | Mea. | 3.28-3.41 | 3.29-3.42 | -20.9 |

isolators are designed and implemented on the top and bottom interfaces of the upper substrate, respectively. The dimensions of the top isolator are a1-l1, and the dimensions of the bottom isolator are a2-l2. These parameters are defined in the same way as in Fig. 3. This means that up to 24 parameters need to be optimized, see Table V. With PSADEA, this task was performed with the constraints and targets as shown in Table VI. After 930 parallel EM simulations (3 designs in parallel in each iteration), all targets were reached. The overall design time was about 61.4 hours.

The frequency reconfigurable antenna array with the proposed isolator was prototyped, see Fig. 8. All the substrates were fixed by nylon screws, which have very limited effect on the antenna array performance, according to simulations.

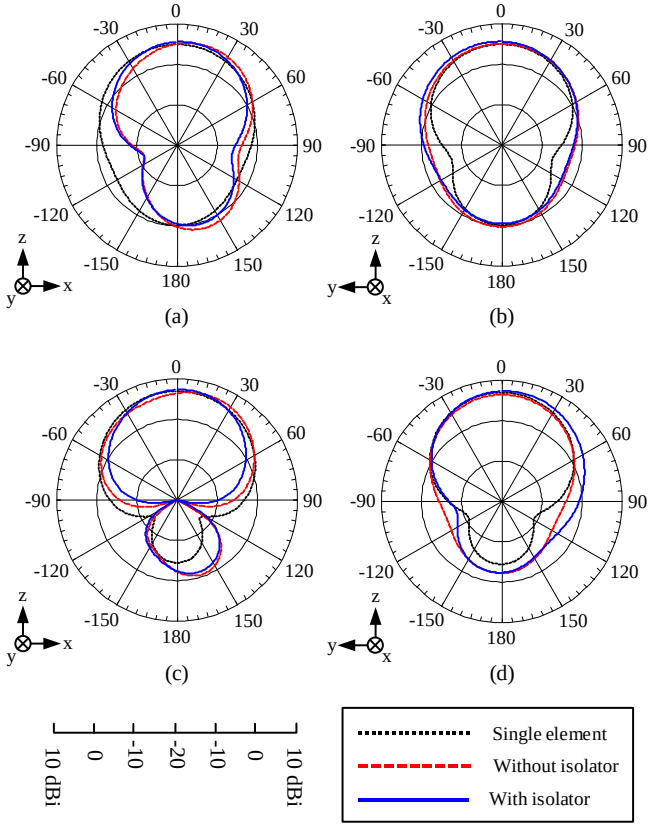


Fig. 10. Radiation patterns of the proposed frequency reconfigurable antenna array. (a) State 1, xz plane, (b) State 1, yz plane, (c) State 2, xz plane, (d) State 2, yz plane. (Abs values of the farfield directivity.)

The S-parameters were measured with an HP 8510 Vector Network Analyzer, and are compared with the simulations in Fig. 9, showing an excellent agreement. The array with the proposed isolator is compared with the single antenna element and the array without isolator in Table VII. The mutual coupling is reduced by -8 dB and -7 dB in the lower band and higher band, respectively with the inclusion of the isolator. The simulated radiation patterns are shown in Fig. 10. The directivities of the embedded element with isolator are 5.75 dBi and 7.43 dBi in State 1 and State 2, respectively, while the corresponding values for the single element are 5.01 dBi and 7.01 dBi, respectively. The radiation efficiencies of the embedded element with isolator are 50 % and 70 % in State 1 and State 2, respectively, while the corresponding values for the single element are 57 % and 72 %, respectively.

## V. CONCLUSION

A surrogate model-assisted global optimization-driven design of mutual-coupling-reducing isolators was proposed. More specifically, the PSADEA algorithm was used. The technique was applied to two 2-element antenna arrays, a ZOR-based array and a frequency reconfigurable array. For the ZOR-based array, the proposed AI-driven method was demonstrated to be more efficient than a traditional experience-driven design method. For the complex frequency reconfigurable array, a parasitic element-based isolator was designed operational in the two bands for the first time. The advantages compared to traditional experience-driven design methods were thus clearly shown. It is important to emphasize that the technique proposed in this communication paves the way to automatically design not only isolators, but also other electromagnetic structures.

## REFERENCES


[1] J. Zhang, S. Yan, and G. A. E. Vandenbosch, "Realization of dual band pattern diversity with a CRLH-TL inspired reconfigurable metamaterial," *IEEE Trans. Antennas Propag.*, vol. 66, no. 10, pp. 5130-5138, Oct. 2018.

[2] D.-B. Hou, S. Xiao, B.-Z. Wang, L. Jiang, J. Wang, and W. Hong, "Elimination of scan blindness with compact defected ground structures in microstrip phased array," *IET Microw. Antennas Propag.*, vol. 3, no. 2, pp. 269-275, Mar. 2009.

[3] J. Ouyang, F. Yang, and Z. M. Wang, "Reducing mutual coupling of closely spaced microstrip MIMO antennas for WLAN application," *IEEE Antennas Wireless Propag. Lett.*, vol. 10, pp. 310–313, 2011.

[4] Z. Iluz, R. Shavit, and R. Bauer, "Microstrip antenna phased array with electromagnetic bandgap substrate," *IEEE Trans. Antennas Propag.*, vol. 52, no. 6, pp. 1446–1453, Jun. 2004.

[5] F. Yang, and Y. Rahmat-Samii, "Microstrip antennas integrated with electromagnetic band-gap (EBG) structures: A low mutual coupling design for array applications," *IEEE Trans. Antennas Propag.*, vol. 51, no. 10, pp. 2936-2946, Oct. 2003.

[6] E. Rajo-Iglesias, Ó. Quevedo-Teruel, and L. Inclan-Sanchez, "Planar soft surfaces and their application to mutual coupling reduction," *IEEE Trans. Antennas Propag.*, vol. 57, no. 12, pp. 3852-3859, Dec. 2009.

[7] Ó. Quevedo-Teruel, L. Inclan-Sanchez, and E. Rajo-Iglesias, "Soft surfaces for reducing mutual coupling between loaded PIFA antennas," *IEEE Antennas Wireless Propag. Lett.*, vol. 9, pp. 91-94, 2010.

[8] Z. Li, Z. Du, M. Takahashi, K. Saito, and K. Ito, "Reducing mutual coupling of MIMO antennas with parasitic elements for mobile terminals," *IEEE Trans. Antennas Propag.*, vol. 60, no. 2, pp. 473-481, Feb. 2012.

[9] S. Farsi, H. Aliakbarian, D. Schreurs, B. Nauwelaers, and G. A. E. Vandenbosch, "Mutual coupling reduction between planar antennas by using a simple microstrip U-section," *IEEE Antennas Wireless Propag. Lett.*, vol. 11, pp. 1501-1503, 2012.

[10] A. C. Durgun, C. A. Balanis, C. R. Birtcher, H. Huang, and H. Yu, "High-impedance surfaces with periodically perforated ground planes," *IEEE Trans. Antennas Propag.*, vol. 62, no. 9, pp. 4510-4517, Sep. 2014.

[11] J. Y. Lee, S. H. Kim, and J. H. Jang, "Reduction of mutual coupling in planar multiple antenna by using 1-D EBG and SRR structures," *IEEE Trans. Antennas Propag.*, vol. 63, no. 9, pp. 4194–4198, Sep. 2015.

[12] J. Zhang, S. Yan, X. Hu, and G. A. E. Vandenbosch, "Mutual coupling suppression for on-body multi-antenna systems," *IEEE Trans. Electromagn. Compat.*, early access.

[13] Z. Li, Z. Du, M. Takahashi, K. Saito, and K. Ito, "Reducing mutual coupling of MIMO antennas with parasitic elements for mobile terminals," *IEEE Trans. Antennas Propag.*, vol. 60, no. 2, pp. 473-481, Feb. 2012.

[14] U. Ullah, I. B. Mabrouk, and S. Koziel, "Enhanced-performance circularly polarized MIMO antenna with polarization/pattern diversity," *IEEE Access*, vol. 8, pp. 11887-11895, 2020.

[15] M. Aziz ul Haq, and S. Koziel, "Feedline alterations for optimization-based design of compact super-wideband MIMO antennas in parallel configuration," *IEEE Antennas Wireless Propag. Lett.*, vol. 18, no. 10, pp. 1986-1990, Oct. 2019.

[16] B. Liu, M. O. Akinsolu, N. Ali, and R. Abd-Alhameed, "Efficient global optimisation of microwave antennas based on a parallel surrogate model assisted evolutionary algorithm," *IET Microw. Antennas Propag.*, vol. 13, no. 2, pp. 149-155, Feb. 2019.

[17] M. O. Akinsolu, B. Liu, V. Grout, P. I. Lazaridis, M. E. Mognaschi, and P. Di Barba, "A parallel surrogate model assisted evolutionary algorithm for electromagnetic design optimisation," *IEEE Trans. Emerg. Topics Comput. Intell.*, vol. 3, no. 2, pp. 93-105, Apr. 2019.

[18] B. Liu, H. Aliakbarian, Z. Ma, G. A. E. Vandenbosch, G. Gielen, and P. Excell, "An efficient method for antenna design optimization based on evolutionary computation and machine learning techniques," *IEEE Trans. Antennas Propag.*, vol. 62, no. 1, pp. 7-18, Jan. 2014.

[19] B. Liu, S. Koziel, and N. Ali, "SADEA-II: a generalized method for efficient global optimization of antenna design," *J. Comput. Design Eng.*, vol. 4, no. 2, pp. 86-97, Apr. 2017.